Purinergic Signaling Participates in a Transition Between Functional States of Reactive Microglia and Controls Astrocyte-Driven Neuroinflammation in the Model of Trimethyltin-Induced Neurodegeneration

Milorad Dragić
Univerzitet u Beogradu Biloski Fakultet
Nataša Mitrović
University of Begrade Vinca Institute of Nuclear Sciences
Marija Adžić
Univerzitet u Beogradu Biloski Fakultet
Nadežda Nedeljković
Univerzitet u Beogradu Biloski Fakultet
Ivana Grković (istanojevic@vin.bg.ac.rs)
University of Belgrade Vinca Institute of Nuclear Science https://orcid.org/0000-0003-4476-7871

Research article

Keywords: hippocampus, neurodegeneration, purinergic receptors, microglial polarization, NTPDase1/CD39, eN/CD73, astrocyte-derived inflammation

Posted Date: December 29th, 2020

DOI: https://doi.org/10.21203/rs.3.rs-135545/v1

Abstract

Background

The present study aims to explore the involvement of purinergic signaling in the rodent model of hippocampal degeneration induced by trimethyltin (TMT), which results in behavioral and neurological dysfunction similar to Alzheimer's disease. Our study has provided novel evidence that TMT induced extracellular depositions of amyloid β, which might be the cause of the well-defined progressive hippocampal neurodegeneration and gliosis.

Methods

We have applied enzyme histochemistry and immunohistochemistry to study spatial and temporal patterns of ectonucleotidase NTPDase1/CD39 and eN/CD73 expression, gene expression analysis and immunochemistry to analyze cellular localization of select purinoreceptors and pro-inflammatory cytokines previously associated with microglia and astrocytes activation.

Results

Our study demonstrated that all Iba1-*ir* microglial cells, irrespective of the cell shape and localization, upregulated NTPDase1/CD39, while the induction of eN/CD73 has been observed only at amoeboid microglia, localized within the hippocampal layers with pronounced cell death. Marked induction of $P2Y_{12}R$ and $P2Y_6R$ at amoeboid microglia might reflect the transition from rod to amoeboid microglia and the adaptation to the migratory and phagocytic properties of the latter. Based on the expression of the microglial polarization markers, the majority of microglia belonged to the M2-like functional state. A significant change in purinergic signaling components accompanied the response of reactive astrocytes, which occupied the areas with pronounced cell death. Reactive astrocytes, which markedly expressed adenosine A_{2A} and $P2Y_1$ receptors, showed massive induction of complement component C3, NF-kB and IL-1β, suggesting that astrocyte-derived inflammation might be responsible for prolonged and spreading neurodegeneration in TMT model.

Conclusion

This study put glia-associated purinergic signaling in the center of molecular pathogenesis of AD-like disease. Our findings suggest that the ectonucleotidases and purinergic signaling play significant role in microgliosis, astrocyte-driven neuroinflammation and prolonged neurodegeneration in the TMT model.

Background

Glial cells are a heterogeneous class of cells in the central nervous system (CNS), playing a range of roles in the maintenance of tissue homeostasis. Among them, critical roles of microglia and astrocytes are to monitor, maintain and preserve the metabolic and structural integrity of the CNS and to respond to noxious stimuli and insults to the brain [1]. Microglial cells react to deranged CNS homeostasis by

immediate changes in their morphology and function, which may progress in two directions, assigned as M1/M2 polarization states. The so-called classical or M1 activation is induced by activation of the classical complement cascade and interferon-γ (IFN-γ), featuring the massive release of pro-inflammatory cytokines, including tumor necrosis factor-α (TNF-α), interleukin (IL)-1β and IL-6, the induction of nitric oxide synthase-2 (iNOS) and the burst of reactive oxygen species (ROS) [2]. Alternatively, microglia may assume a neuroprotective M2 phenotype, characterized by elevated expression of anti-inflammatory cytokines, such as transforming growth factor β (TGF-β) and IL-10, and the induction of molecular markers, like arginase-1 (Arg1) [3], [4]. The M2 microglial cells clear apoptotic bodies, and refine synapses through phagocytosis [5] and release protective factors, which may contribute to protection and repair. The M1/M2 represents two extreme activation phenotypes of reactive microglia, with a full repertoire of transitional states between them. Based on a distinct combination of microenvironment influences, alternatively activated microglia may be categorized into the subsets termed M2a, M2b, M2c, M2d microglia [6], capable to perform specific functions in different physiological and pathological conditions [7]. In response to brain injury, astrocytes assume reactive states that may be discriminated based on the proliferation, and induction of pro-inflammatory mediators and ROS to: (i) newly proliferated astrocytes organized to forms borders around areas of tissue damage or inflammation, and (ii) non-proliferative astrocytes that retain the basic cell structure, tissue architecture, and functional interactions established in healthy tissue. With the analogy to reactive states of microglia, based on their molecular signature these two broad reactive astrocyte subtypes are also classified as A1 pro-inflammatory and A2 anti-inflammatory astrocytes [8].

Microglia and astrocytes communicate with each other and with affected neurons by using a range of paracrine signals, including cytokines, gliotransmitters, and neuromodulators. When exposed to noxious stimuli the glial cells become a major source of adenosine triphosphate (ATP), released through the hemichannels [9], [10]. The nucleotide acts as a “danger signal” [11] via two classes of purinergic receptors, i.e. ligand-gated P2X channels and G-protein coupled P2Y receptors, widely expressed at all CNS cell types. ATP promotes microglial chemotaxis towards the challenged area [4], [12] via $P2Y_{12}$ receptors [13] and triggers microglial phagocytosis through activation of the $P2Y_6$ receptor [14]. Furthermore, ATP promotes the release of pro-inflammatory cytokines IL-1β, TNF-α, and IFN-γ via $P2X_7$ receptors [15] and induces the astrocytic release of cytokines/chemokines and glia-derived neurotrophic factor (GDNF) via $P2Y_1R$ [4]. The reach and duration of extracellular ATP actions are tightly regulated by membrane-bound ectonucleotidases, which rapidly hydrolyze ATP, by its sequential hydrolysis to adenosine, as the final product. Adenosine, on the other hand, mainly exerts anti-inflammatory and immunosuppressive effects, via G-protein coupled adenosine receptors (A_1R, $A_{2A}R$, $A_{2B}R$, and A_3R) [16], [17].

The enzymatic breakdown of extracellular ATP and the generation of adenosine are catalyzed by two functionally coupled ectonucleotidases, namely ectonucleoside triphosphate diphosphohydrolase 1 (NTPDase 1/CD39) and ecto-5' nucleotidase (eN/CD73) [18]–[20]. In the CNS, NTPDase1/CD39, largely expressed at microglia and vascular endothelial cells [11], [21], crucially participates in the regulation of

P2X and P2Y receptor signaling, via hydrolysis of ATP and ADP. The resulting AMP is hydrolyzed to adenosine by eN/CD73, which is expressed by neurons, glial cells, ependymal cells, and cells of the choroid plexus [18], [20], [21]. The two ectonucleotidases act together as an immune checkpoint, as they determine the ratio of ATP/adenosine and the inflammatory status of the tissue. Accordingly, altered function of NTPDase1/CD39 and eN/CD73 and the dysregulation of the purinergic signaling are largely implicated in the pathophysiology of several neurological diseases, including Alzheimer's disease (AD), Parkinson disease (PD), multiple sclerosis (MS), and astroglioma [22]. Therefore, NTPDase1/CD39 and eN/CD73 represent promising pharmacological targets in the treatment and control of neuroinflammatory processes [23].

The main goal of the present study is to explore the involvement of ectonucleotidases and purinergic signaling in the rodent model of hippocampal degeneration induced by trimethyltin (TMT). The toxicant induces a selective and progressive hippocampal neurodegeneration and chronic microgliosis and astrogliosis, which result in behavioral and neurological symptoms and memory dysfunction similar to AD [24]–[27]. In the previous paper, we have described particular reactive astrocyte phenotypes and their dynamic remodeling in TMT-induced neurodegeneration [28]. The TMT-induced reactive astrocyte phenotypes have been previously linked with increased activation of glial $P2X_2R$ [29]. Given that the involvement of purinergic signaling has not been explored in the TMT model, in the present study, we have analyzed the spatial and temporal patterns of NTPDase1/CD39 and eN/CD73 and purinergic receptors expression in the context of microglia and astrocytes activation.

Materials And Methods

Animals, surgical procedure and treatment

Two-month old female rats of the Wistar strain (200 – 220 g) maintained in the animal facility of the VINČA Institute of Nuclear Sciences - National Institute of Republic of Serbia, University of Belgrade were used in the study. Appropriate actions were taken to alleviate the pain and discomfort of the animals in accordance with the compliance with European Communities Council Directive (2010/63/ EU) for animal experiment, and the research procedures were approved by the Ethical Committee for the Use of Laboratory Animals of VINČA Institute of Nuclear Sciences - National Institute of Republic of Serbia, University of Belgrade, Belgrade, Republic of Serbia (Application No. 323-07-02057/2017-05 and No. 323-07-04787/2019-05). Animals were housed 3-4/cage, in a 12 h light/dark regime, constant humidity and temperature, and free access to food and water.

It was previously shown that TMT induced hippocampal neurodegeneration and gliosis, the pattern of which was comparable in adult rats of both sexes [24]–[26], [28], [30], [31]. However, given that the expression of ectonucleotidases in the brain is under the control of gonadal steroids and differs in two sexes [21], [32], [33], the study was performed in female rats, bilaterally ovariectomized three weeks prior to TMT injection [28].

A total of 80 animals were divided into two groups. On day zero, animals of TMT group received TMT (8 mg/kg dissolved in 1 mL 0.9 % w/v saline) (in the form of a single *i.p* injection), whereas the control group received the adequate volume of 0.9 % saline solution. The animals were returned to their cages and monitored for unusual signs of behavior until sacrifice. At 2-, 4-, 7- and 21-days post-intoxication (dpi), animals of TMT and control groups (10 animals/group) were sacrificed by decapitation (Harvard apparatus, Holliston, MA, USA).

Histochemistry, immunohistochemistry and immunofluorescence microscopy

Brains (n = 5 per group) were carefully removed from the skull, fixed in 4 % PFA for 24 hours, cryoprotected in graded sucrose (10-30 % in 0.2 M phosphate buffer), and stored at 4°C, as described before [21], [28]. The brains were cryosectioned in serial 25-μm thick coronal sections and the sections at 3.12 – 3.84 mm antero-posterior to Bregma were air-dried and stored at – 20°C until use.

Nissl staining

Alterations in hippocampal cytoarchitecture induced by TMT injection were evaluated by Nissl staining. Sections were kept in 0.5 % thionine solution for 20 min, washed in tap water, dehydrated in graded ethanol (70 % - 100 %), and cleared in xylene for 2×5 min and covered with DPX-mounting medium (Sigma Aldrich, USA).

Immunohistochemistry and immunofluorescence

Slides were kept at room temperature (RT) for 30 min prior to staining. After washing in PBS, slides were put in 0.3 % H_2O_2 in methanol for 20 min, to block endogenous peroxidase, and then immersed in 5 % donkey normal serum at RT for 1 h to block a non-specific binding. Sections were probed with primary antibodies, overnight at 4°C in a humid chamber. After washing in PBS (3×5min), sections were incubated with horseradish peroxidase (HRP)-conjugated secondary antibodies (2 h, RT in a humid chamber). The list of antibodies used for immunohistochemistry (ICH) and immunofluorescence (IF) is presented in Table 1. The immunoreaction was visualized with 3,3´S-diaminobenzidine-tetrahydrochloride (DAB, Abcam, UK), which is converted to the insoluble brown precipitate by HRP. Sections were washed in distilled water, dehydrated in graded ethanol solutions (70 % - 100 %), cleared in xylene, and mounted with the use of DPX-mounting medium (Sigma Aldrich, USA). Sections were analyzed under LEITZ DM RB light microscope (Leica Mikroskopie & Systems GmbH, Wetzlar, Germany), equipped with LEICA DFC320 CCD camera (Leica Microsystems Ltd., Heerbrugg, Switzerland) and LEICA DFC Twain Software (Leica, Germany). All images were captured at 40× magnification.

The identical protocol has been applied for double and triple immunofluorescence (IF) staining, with the omission of the methanol/H_2O_2 step. After incubation with primary antibodies (Table 1), sections were probed with fluorescence-dye labeled secondary antibodies and mounted with Mowiol (Calbiochem, La Jolla, CA). For double and triple IF staining, primary and secondary antibodies were separately applied for each labeling. Sections incubated without primary antibodies or with rat pre-immune sera were used as

negative controls. Sections were analyzed by confocal laser-scanning microscope (LSM 510, Carl Zeiss GmbH, Jena, Germany), using Ar Multi-line (457, 478, 488 and 514 nm), HeNe (543 nm) and HeNe (643 nm) lasers using 63× (×2 digital zoom) DIC oil, 40× and monochrome camera AxioCam ICm1 camera (Carl Zeiss GmbH, Germany).

Enzyme histochemistry

Ectonucleotidase enzyme histochemistry based on the ATP/ADP-, and AMP-hydrolyzing activities of NTPDase1/CD39 and eN/CD73, respectively have been applied [21], [34]. Briefly, cryosections were preincubated for 30 min at RT in TRIS-maleate sucrose buffer (TMS), containing 0.25 M sucrose, 50 mM TRIS-maleate, 2 mM $MgCl_2$ (pH 7.4), and 2 mM levamisole, to inhibit tissue non-specific alkaline phosphatase. The enzyme reaction was carried out at 37 °C/60 min, in TMS buffer, containing 2 mM $Pb(NO3)_2$, 5 mM $MnCl_2$, 3 % dextran T250, and 1 mM substrate (ATP, ADP or AMP), as substrate. After thorough washing, slides were immersed in 1% (v/v) $(NH_4)_2S$, and the product of enzyme reaction was visualized as an insoluble brown precipitate at a site of the enzyme activity. After dehydration in graded ethanol solutions (70-100 % EtOH, and 100% xylol), slides were mounted with a DPX-mounting medium (Sigma Aldrich, USA). The sections were examined under LEITZ DM RB light microscope (Leica Mikroskopie & Systems GmbH, Wetzlar, Germany), equipped with LEICA DFC320 CCD camera (Leica Microsystems Ltd., Heerbrugg, Switzerland) and analyzed using LEICA DFC Twain Software (Leica, Germany).

Immunofluorescence quantification

Raw multi-image immunofluorescence micrographs were used to measure integrated fluorescence density and the density confined within five pre-defined regions of interest (ROIs), with background fluorescence subtraction for at least 3 images per ROI and n = 5 sections per group (JACoP ImageJ plugin). A degree of overlap and correlation between multiple channels were estimated by calculating Pearson's correlation coefficient (PCC) [35]. PCC is statistical parameter that reflects both co-occurrence (degree at which intensities of two channels for each pixel are beyond or above the threshold), and correlation (pixel-for pixel proportionality in the signal levels of the two channels). PCC values range from 1 (for two images whose fluorescence intensities are perfectly, linearly related) to - 1 (for two images whose fluorescence intensities are perfectly, but inversely, related to one another). Values near zero reflect distributions of probes that are uncorrelated with one another. The results are expressed as mean PCC± SEM.

Gene expression analysis by RT-qPCR and statistical analysis

Total RNA was extracted from the hippocampal formation (2-, 4-, 7-, 21-dpi and appropriate controls, n = 5 per group) using TRIzol Reagent (Invitrogen, Carlsbad, CA, USA), according to the manufacturer's instructions. Purity and the concentration of isolated RNA were assessed by OD 260/OD280 and OD260, respectively. Complementary DNA (cDNA) was synthesized using High-Capacity cDNA Reverse Transcription Kit (ThermoFisher Scientific, MA, USA) and stored at – 20°C until use. Quantitative real-time

PCR was performed using Power SYBR™ Green PCR Master Mix (Applied Biosystems, MA, USA) and ABI Prism 7000 Sequence Detection System (Applied Biosystems, MA, USA) under the following conditions: 10 min of enzyme activation at 95 °C, 40 cycles of 15 s denaturation at 95 °C, 30 s annealing at 60 °C, 30 s amplification at 72 °C, and 5 s fluorescence measurement at 72 °C. Primer sequences used for the amplification are given in Table 2. Relative quantification was performed using $2^{-\Delta\Delta Ct}$ method, using cyclophilin A (CycA), as a reference gene. For each group, five samples run in duplicate were analyzed. Amplification efficacy was assessed by the generation of internal standard curves by several-fold dilutions of generated cDNA, while melting curve analysis at the end of each experiment was used to confirm the formation of a single PCR product. The results were expressed as the abundance of target mRNA/CycA-mRNA at each dpi relative to a corresponding intact control ± SD. The mRNA levels of most investigated genes showed biphasic response to TMT intoxication; initial downregulation at 2-dpi was followed with gradually upregulation and overcoming basal levels at 7- and 21-dpi (Supplementary Table 1). The transient down-regulation may be the consequence of increased corticosterone levels [36] observed in the days after TMT intoxication [37], [38].

Statistical analysis

Quantitative data were scrutinized for normality and statistically analyzed by parametric tests. The results of qPCR and PCC quantification obtained for 7-dpi and 21-dpi were compared to the corresponding control and analyzed using Student's *t-test*. Data are presented as mean ± S.E.M. For all statistical analyses, Graphpad Prism 5.04 (Graphpad) software was used.

Results

Spatio-temporal patterns of neurodegeneration, amyloid-β deposition and gliosis after TMT exposure

Nissl staining, applied to explore the overall hippocampal cytoarchitecture, corroborated existing data on TMT-induced neurodegeneration (Figure 1). Briefly, cell disorganization and thinning of neuronal cell layers in CA1 and hilus/pCA3 observed already at 4-dpi, progressed to noticeable neurodegeneration in CA1 and proximal and medial CA3 (p/mCA3) at 7-dpi (Figure 1*a*), with almost complete disappearance of neuronal somata in CA1 and p/mCA3 regions at 21-dpi. Of note is that during the whole period after TMT exposure, the complete CA2 sector remained intact, without apparent neuronal cell loss and gliosis. On the top of cell death, immunolabeling directed to amyloid-β protein (Aβ) demonstrated the presence of Aβ depositions in neuronal cell layers of CA1 and CA3, in the form of diffuse and dense-core plaques, at 7-dpi and 21-dpi, respectively (Figure 1*b*). Immunostaining directed to astrocyte marker GFAP showed the presence of pronounced gliosis (Figure 1*c*). The first indication of astrogliosis was observed already at 2-dpi [28] while the full-blown hypertrophied astrocytes were seen at 7-dpi in CA1 region and atrophy-like morphotype was observed in the hilar/CA3 region. At 21-dpi, hypertrophied/atrophied astrocytes were widespread in CA1 and CA3 sectors, and covered the hilar region in the form of gliotic scar, while CA2 remained devoid of GFAP-*ir*. Even greater diversity in cell morphology was observed among reactive microglia (Figure 1*e*). Specifically, highly ramified Iba1-*ir* cells, evenly distributed in the control

hippocampal tissue (Figure 1*d*), were gradually transformed to peculiar rod Iba1-*ir* cells at 4-dpi, observed in synaptic layers of CA1 and the hilar/pCA3. Besides rod shape, a range of other reactive Iba1-*ir* morphotypes was observed, from hyper-ramified to bushy/amoeboid. At 7-dpi, more rod Iba1-*ir* cells populated the synaptic layers in the entire CA1 and the hilar/pCA3 sectors, while cells which already entered neuronal cell layers, attained amoeboid morphology. At 21-dpi, Iba1-*ir* cells located just next to neuronal cell layers still displayed their elongated morphology, while more numerous Iba1-*ir* in neuronal cell layers displayed amoeboid morphology. Interestingly, rod Iba1-*ir* cells were not observed in the hilar/pCA3, whereas at the latest time point, the hilar area and granular cell layer appeared completely without Iba1-*ir* (Figure 1*d*).

Expression of NTPDase1/CD39, eN/CD73 and purinoreceptors involved in microglial reactivity

The main goal of the present study was to explore the involvement of the purinergic signaling system in the TMT-induced hippocampal neurodegeneration and gliosis. Gene expression analyses included genes encoding NTPDase1/CD39 and eN/CD73, which are the major ectonucleotidases involved in the extracellular catabolism of ATP in the brain. Two and a half- and five-fold increase in NTPDase1/CD39-mRNA abundance were observed at 7-dpi and 21-dpi, respectively, and two-fold increase in eN/CD73-mRNA was observed at 21-dpi (Figure 2*a*). The identity of cells that up-regulate NTPDase1/CD39 in response to TMT was determined by enzyme histochemistry, which enables labeling of cells that exhibit the enzymatic activity *in situ*. In control sections, the product of ATP/ADP-hydrolyzing reactions, which corresponded to the catalytic activity of NTPDase1/CD39, was uniformly present at ramified cells that, based on morphological criteria, belonged to resting microglia (Figure 2*b*). At 7-dpi, cells with ovoid cell body and retracted process, in the vicinity or within neuronal cell layers were histochemically labeled. At 21-dpi, numerous amoeboid cells infiltrated the neuronal cell layers. The obtained patterns of ATP/ADP enzyme activities closely corresponded to Iba1-*ir* (Figure 1*d*), suggesting that reactive microglial cells mostly up-regulated NTPDase1/CD39 after the exposure to TMT.

The identity of cells that induced eN/CD73 in response to TMT was determined by combining AMP-based enzyme histochemistry (Figure 2*b*) with eN/CD73-directed immunocytochemistry (Figure 2*c*). In intact hippocampal tissue, diffuse histochemical reaction and eN/CD73-*ir* were observed in synaptic layers, while neuronal cell layers remained unstained. After TMT exposure, the histochemical reaction and eN/CD73-*ir* begun to be noticed at amoeboid cells, increasingly infiltrating within neuronal cell layers from 7-dpi and afterwards. Cellular localization of eN/CD73-*ir* was ascertained by triple immunofluorescence directed to GFAP, Iba1, and eN/CD73 (Figure 3*a*). The pattern of eN/CD73-*ir* increasingly overlapped with Iba1-*ir*, peaking at 21-dpi at amoeboid Iba1-*ir* cells infiltrated within neuronal cell layers, while the co-localization with GFAP-*ir* was not observed. These findings confirmed the dominant expression and up-regulation of eN/CD73 by reactive microglial cells after TMT exposure. The co-localization of NTPDase1/CD39 and eN/CD73 at microglial cells was demonstrated by double-immunofluorescence labeling, which showed the overlap of the signals corresponding to NTPDase1/CD39 and eN/CD73 at amoeboid microglial cells, while ramified and rod NTPDase1/CD39-*ir* cells within synaptic layers did not show eN/CD73-*ir* (Figure 3*b*). The level of overlap between the two-*ir*

signals was quantified by using Pearson correlation coefficient (PCC). The raising PCC values showed increasing overlap between Iba-1/eN/CD73-*ir* and NTPDase1/CD39-eN/CD73-*ir* signals after TMT exposure, whereas negative PCC values for GFAP-*ir* and eN/CD73-*ir* corroborated the lack of astrocytic expression of eN/CD73 after TMT.

We further assessed gene expression of several purinoceptors functionally associated with chronic neuroinflammation (Figure 4). Concerning ATP/ADP–sensitive P2 receptors, we detected strong up-regulation of $P2X_4R$-, $P2X_7R$- and $P2Y_2R$-mRNA and almost 20-fold induction of $P2Y_6R$- and $P2Y_{12}R$-mRNA at 7-dpi and 21-dpi. For P1 receptors, a several-fold increase in A_3R-mRNA at 7-dpi and 21-dpi, together with significant, but less conspicuous induction of A_1R-, $A_{2A}R$- and $A_{2B}R$-mRNAs were detected at the latest time point after TMT exposure.

Functional state of reactive microglia and astrocytes

The results pointed to the marked induction of NTPDase1/CD39 by microglial cells, and the co-localization with eN/CD73 at amoeboid microglial cells after TMT exposure. It is known that resting microglia activate under the influence of ATP and develop functional phenotype, which may be broadly categorized as pro-inflammatory or neuroprotective. Therefore, we next assessed the inflammatory status of the tissue, by determining the expression of several cytokines and inflammation markers, iNOS, C3, and arginase 1 (Arg1), which are often used to discriminate between M1/M2 polarization states. Several-fold increases in TNF-α- and IL-6-mRNA abundances at 7-dpi at the earliest, followed by strong up-regulation of IL-1β- and IL-10-mRNA (Figure 5*a*) at the latest time point were detected. The induction of the cytokines was accompanied by prominent and lasting induction of C3-mRNA and iNOS-mRNA (Figure 5*a*), without significant change in Arg1-mRNA (data not shown). However, neither of the tested pro-inflammatory cytokines (data not shown) and polarization markers was found in association with Iba1-*ir*, as demonstrated by double immunofluorescence (Figure 5*b*). However, Iba1-*ir* cells did show Arg1-*ir* and *ir* corresponding to phagocytic marker CD68. The signals co-occurrence was observed at rod and amoeboid cells at 7-dpi and later. The induction of the chemotaxis marker $P2Y_{12}R$ was also observed at Iba1-*ir* cells.

The lack of expression of pro-inflammatory cytokine and markers by Iba1-*ir* microglial cells prompted us to explore their astroglial expression (Figure 6). Specifically, the signals corresponding to IL-1β, TNF-α, and IL-10 almost completely overlapped with GFAP-*ir* at 7-dpi and 21-dpi. The GFAP-*ir* cells also expressed iNOS, NF-kB, and C3, suggesting that the astrocytes were the major source of the inflammatory cytokines and the driving force of the TMT-induced neuroinflammation. With regard to purinoreceptors expression, massive induction of $P2Y_1R$ and $A_{2A}R$ was found on GFAP-*ir* and C3-*ir* astrocytes at 7-dpi and 21-dpi, which suggested the involvement of the purinoreceptors in the pro-inflammatory astrocyte phenotype.

Discussion

The results of the present study corroborate the existing data on the spatiotemporal pattern of neurodegeneration and gliosis in the TMT model. Briefly, a single *i.p.* injection of TMT triggered a wave of spreading neurodegeneration and neuronal cell death starting from 2-dpi, which sequentially hit neuronal cell layers of the hilus/CA3, and CA1, while sparing the entire CA2 sector [24], [26], [28], [39]. As a result of the neuronal cell death, the entire affected sectors became gradually populated with reactive astrocytes, whose number and hypertrophy became noticeable at 4-dpi and peaked at 21-dpi, while the response of microglia slightly lagged behind. Again, the hardest hit neuronal cell layers in hilus/CA3, and CA1 sequentially became infiltrated with microglial cells of amoeboid shape, while the CA2 neuronal cell layer rested spared. Synaptic layers in the affected sectors became largely populated with rod microglia, occasionally found in a train formation. At the end of the monitoring period, hilus/CA3 was completely devoid of microglia, while the parenchyma was covered with numerous astrocytes with atrophic-like morphology [28].

On top of the neurodegeneration, the present study provided the novel evidence that TMT caused extracellular depositions of Aβ, implying that it might play a role in TMT-induced neurodegeneration, as shown in AD and several other diseases, including PD, Huntington's disease and posttraumatic brain [40]. By analogy with AD, we hypothesize that Aβ may trigger neuroinflammatory responses of microglia and astrocytes by enhancing the release of ATP and the activation of ATP-sensitive purinoceptors [41], [42]. Degradation of extracellular ATP results in extracellular adenosine level jump and enhanced adenosine receptor-mediated responses [42], which set the inflammatory status of the tissue [17]. Therefore, the present study aimed to explore the supposed parallels between the TMT model and AD, with special reference to purinergic signaling and its role in gliosis.

Keeping up with the main goal, the central finding of our study is prominent induction of NTPDase1/CD39 and eN/CD73 by reactive microglial cells after TMT exposure, whereas the pattern of the induction differed between two main morphotypes of reactive microglial cells. In physiological conditions, resting microglia express NTPDase1/CD39 [43]. After the exposure, NTPDase1/CD39 was markedly up-regulated in all Iba1-*ir* cells, irrespective of their shape and position, while eN/CD73 was selectively up-regulated in distinct microglial cell type. Specifically, eN/CD73 was expressed by amoeboid Iba1-*ir* cells, implicating that the differential induction might be an adaption to specific hippocampal micro-location or specific function of the microglial subsets. The transition between functional states of reactive microglia is accompanied by the morphological transformation of the cells, and among the critical factors that trigger the transition are ATP, adenosine, vitamin E, IL-34, and chemokine fractalkine [44]–[46]. Rod microglia are usually found at early stages in AD, in association with damaged neurons and axons, and not in aggregation with other glial cells [5], which imply their protective and reparative role [47]. Rod cells are able to provide new cells and to transform into amoeboid microglia [48]. Hence, the main functional properties of amoeboid microglia are motility and phagocytosis, both of which are tightly regulated by purinergic signaling mediated by NTPDase1/CD39 and eN/CD73 and select P1 and P2 receptors [19]. Specifically, adenosine controls the retraction of microglial processes and the shape change via A_{2A}Rs [49], and affects chemotaxis via $P2Y_{12}R/A_3R$ co-activation [13], [50]. The activation of

the purinoceptors, specifically the activation of $P2Y_6R$ in microglial cells promotes the phagocytosis of debris generated by excitotoxic hippocampal damage [51]. Furthermore, NTPDase1/CD39 and eN/CD73 not only that catabolize extracellular ATP and provide adenosine, but function as clusters of differentiation and cell adhesion molecules, which regulate the adhesion and glial cell migration through specific interactions with extracellular matrix components [52]. Thus, we propose that the up-regulation of NTPDase1/CD39 and eN/CD73 and the change in purinoceptors repertoire induced by TMT are specific adaptations to the phagocytic activity and amoeboid shape of microglial cells, which migrate along with the wave of spreading neurodegeneration, from hilus towards CA3 and CA1.

With regard to the functional state and M1/M2 polarization of microglia, our data showed that Iba1-*ir* cells co-expressed Arg1 and CD68, and did not exhibit iNOS, NF-kB, and C3, which imply the M2-like reactive phenotype [53]. The up-regulation of NTPDase1/CD39 by M2-like microglial cells was previously demonstrated in experimental autoimmune encephalomyelitis, where the induction of NTPDase1/CD39 tended to be associated with Arg1-*ir* and CD68-*ir* microglial cells [54]. M2 polarized microglia may be further divided into four distinct subsets induced by different environmental cues, among which M2d is triggered by IL-6 and develops under the influence of adenosine [53]. Specifically, it has been shown that activation of microglial TLR receptors induces $A_{2A}R$- and $A_{2B}R$-mediated switch in the production of cytokines, from pro-inflammatory TNF-α to the anti-inflammatory IL-10 [53], [55], [56]. Our study provided mechanistic evidence for all the critical steps in the sequential pathway, including induction of IL-6, transcriptional and functional up-regulation of NTPDase1/CD39 and eN/CD73, and induction of $A_{2A}R$ and A_3R. The trend of decreasing expression of TNF-α and IL-6 and increasing expression of IL-10 signaling, presented herein is also in the correlation with M2d reactive microglial state.

Our study also provided evidence that purinergic signaling regulates functional attributes of reactive astrocytes after TMT-induced neurodegeneration as well. Massive induction of $P2X_7R$ at the latest time point after TMT exposure reflected the involvement of the low-affinity ATP receptors in the delayed and lasting astrogliosis initiated by a single TMT injection. It is known that ATP locally released as a danger signal from damaged neurons acts at $P2X_7R$ located at proximal glial cells and initiates NOD-like receptor protein 3 inflammasome assembly and the release of IL-1β [41], [57]. However, a wave of neurodegeneration and apoptosis induced by TMT might provide conditions for a sustained ATP release and prolonged $P2X_7R$ activation, with the resulting postponed induction of IL-1β, together with TNF-α, IL-18, and IL-6 [41]. We have demonstrated that TMT induced IL-1β, not before 21-dpi, primarily in reactive astrocytes which co-expressed markers of the pro-inflammatory phenotype, iNOS, NF-kB, and C3. At the latest time point, these apparently pro-inflammatory astrocytes up-regulated $A_{2A}Rs$, whose aberrant expression was demonstrated in the hippocampal astroglia in AD patients and in AD mouse models [58], [59]. Furthermore, massive induction of $P2Y_1R$ on astrocytes postulates its significance in TMT-induced reactive astrogliosis, as already demonstrated in several models of AD [60], [61]. It is known that pathological conditions may induce gain-of-function in $A_{2A}Rs$ signaling, due to the establishment of toxic iso- and hetero-receptor complexes with other membrane proteins and the disturbance of several intracellular signaling pathways [62]. Moreover, given that eN/CD73 provides the ligand for $A_{2A}R$

activation, enhanced expression of eN/CD73 and the prolonged coupling with $A_{2A}R$ had been suggested to play a role in the transition between acute and chronic neuroinflammation in several neurodegenerative disorders [17], as well it may be the case in AD-like TMT-induced neurodegeneration.

Conclusion

To sum up, our study demonstrates that purinergic signaling plays a significant role in microglial and astroglial responses to TMT-induced neurodegeneration. Marked and distinct changes in eN/CD73 and purinoreceptors expression accompany activation of microglia and their transition towards two prevailing morphotypes, rod and amoeboid microglia. The induction of NTPDase1/CD39, eN/CD73, and select purinoreceptors, most notably $P2Y_{12}$ and $P2Y_6$, probably reflected the transition from rod to amoeboid microglia and the adaptation to the migratory and phagocytic properties of the cells, which, according to the expression of the functional polarization markers, most likely belonged to M2d functional state of the cells. The significant change in purinergic signaling components accompanied the response of reactive astrocytes as well, which permeated the neuronal cell layers in affected sectors. Reactive astrocytes massively up-regulated $A_{2A}R$, together with the persuasive expression of complement component C3, NF-kB, and IL-1β, indicating their harmful phenotype responsible for the prolonged and spreading neurodegeneration. Overall, the results of our study suggest that the ectonucleotidases and purinergic signaling play significant role in microgliosis, astrocyte-driven neuroinflammation and prolonged neurodegeneration in the TMT model (Fig 7).Finally, our results put glia-associated purinergic signaling in the center of molecular pathogenesis of AD-like disease.

Abbreviations

CNS*:* Central nervous system; TMT: trimethyltin; AD: Alzheimer's disease; DAMP: Damage-associated molecular pattern; GFAP: Glial fibrillary acidic protein; IBA1: Ionized calcium binding adaptor molecule 1; CA: Cornu Ammonis;

Declarations

Conflict of interest

The authors declare that they have no conflict of interest.

Ethics approval

The Ethical Committee approved all animal procedures for the Use of Laboratory Animals of "VINČA" Institute of Nuclear Sciences - National Institute of Republic of Serbia, University of Belgrade, Belgrade, Serbia and animals were treated in accordance with the European Community Council Directive of 86/609/ EEC for animal experiment.

Funding

The research was funded by the Ministry of Education, Science and Technological Development of the Republic of Serbia No 0902002 and No 451-03-68/2020-14/200178.

Acknowledgement

The authors thank Professor Jean Sevigny from the Faculté de Médecine, Université Laval, Quebec City, QC, Canada for a kind gift of rabbit anti-rat NTPDase1/CD39 (mN1-2C) and eN/CD73 (rNu-9L) antibodies used in this study. We would also like to thank our Dr. Ivana Bjelobaba, Institute for Biological Research "Siniša Stanković", National Institute of Republic of Serbia, University of Belgrade, Belgrade, Serbia, for providing us with qPCR primers used in this study.

Data availability statement

The data that support the findings of this study are available from the corresponding author upon reasonable request.

Author information

Department for General Physiology and Biophysics, Faculty of Biology, University of Belgrade, Belgrade, Serbia

Milorad Dragić, Marija Adžić, Nadežda Nedeljković

Department of Molecular Biology and Endocrinology, VINČA Institute of Nuclear Sciences-National Institute of the Republic of Serbia, University of Belgrade, Belgrade, Serbia

Nataša Mitrović, Ivana Grković

Center for Laser Microscopy, Faculty of Biology, University of Belgrade, Belgrade, Serbia

Marija Adžić

Contribution

All named authors meet the International Committee of Medical Journal Editors (ICMJE) criteria for authorship for this article. I.G. conceived and directed the projects. M.D. and I.G. designed experiments and performed all histology, analyzed the data and wrote the manuscript. N.M. performed qPCR experiments. M.A. was involved in confocal microscopy and image acquisition. N.N. was involved in data interpretation and wrote the manuscript. All authors had full access to all of the data in this study and take complete responsibility for the integrity of the data and accuracy of the data analysis. All authors read, revised and approved the final manuscript.

References

[1] K. D. Rochfort and P. M. Cummins, “The blood-brain barrier endothelium: a target for pro-inflammatory cytokines.,” *Biochemical Society transactions*, vol. 43, no. 4, pp. 702–706, Aug. 2015.

[2] H. O. Kalkman and D. Feuerbach, “Antidepressant therapies inhibit inflammation and microglial M1-polarization.,” *Pharmacology & therapeutics*, vol. 163, pp. 82–93, Jul. 2016.

[3] H. J. Park, S. H. Oh, H. N. Kim, Y. J. Jung, and P. H. Lee, “Mesenchymal stem cells enhance α-synuclein clearance via M2 microglia polarization in experimental and human parkinsonian disorder.,” *Acta neuropathologica*, vol. 132, no. 5, pp. 685–701, Nov. 2016.

[4] P. Illes, P. Rubini, H. Ulrich, Y. Zhao, and Y. Tang, “Regulation of Microglial Functions by Purinergic Mechanisms in the Healthy and Diseased CNS.,” *Cells*, vol. 9, no. 5, p 1108, Apr. 2020.

[5] M. K. Zabel and W. M. Kirsch, “From development to dysfunction: microglia and the complement cascade in CNS homeostasis.,” *Ageing research reviews*, vol. 12, no. 3, pp. 749–756, Jun. 2013.

[6] T. Rőszer, “Understanding the Mysterious M2 Macrophage through Activation Markers and Effector Mechanisms.,” *Mediators of inflammation*, vol. 2015, p. 816460, 2015.

[7] H. Hirbec, F. Rassendren, and E. Audinat, “Microglia Reactivity: Heterogeneous Pathological Phenotypes.,” *Methods in molecular biology (Clifton, N.J.)*, vol. 2034, pp. 41–55, 2019.

[8] S. A. Liddelow and B. A. Barres, “Reactive Astrocytes: Production, Function, and Therapeutic Potential.,” *Immunity*, vol. 46, no. 6, pp. 957–967, Jun. 2017.

[9] J. A. Orellana *et al.*, “Amyloid β-induced death in neurons involves glial and neuronal hemichannels.,” *The Journal of neuroscience : the official journal of the Society for Neuroscience*, vol. 31, no. 13, pp. 4962–4977, Mar. 2011.

[10] J. A. Orellana *et al.*, “ATP and glutamate released via astroglial connexin 43 hemichannels mediate neuronal death through activation of pannexin 1 hemichannels.,” *Journal of neurochemistry*, vol. 118, no. 5, pp. 826–840, Sep. 2011.

[11] B. Sperlágh and P. Illes, “Purinergic modulation of microglial cell activation.,” *Purinergic signalling*, vol. 3, no. 1–2, pp. 117–127, Mar. 2007.

[12] R. J. Rodrigues, A. R. Tomé, and R. A. Cunha, “ATP as a multi-target danger signal in the brain.,” *Frontiers in neuroscience*, vol. 9, p. 148, 2015.

[13] S. E. Haynes *et al.*, “The P2Y12 receptor regulates microglial activation by extracellular nucleotides.,” *Nature neuroscience*, vol. 9, no. 12, pp. 1512–1519, Dec. 2006.

[14] L.-P. Bernier, A. R. Ase, É. Boué-Grabot, and P. Séguéla, “Inhibition of P2X4 function by P2Y6 UDP receptors in microglia.,” *Glia*, vol. 61, no. 12, pp. 2038–2049, Dec. 2013.

[15] H. Franke, A. Verkhratsky, G. Burnstock, and P. Illes, “Pathophysiology of astroglial purinergic signalling.,” *Purinergic signalling*, vol. 8, no. 3, pp. 629–657, Sep. 2012.

[16] G. Haskó and B. Cronstein, “Regulation of inflammation by adenosine.,” *Frontiers in immunology*, vol. 4, p. 85, 2013.

[17] N. Nedeljkovic, “Complex regulation of ecto-5’-nucleotidase/CD73 and A(2A)R-mediated adenosine signaling at neurovascular unit: A link between acute and chronic neuroinflammation.,” *Pharmacological research*, vol. 144, pp. 99–115, Jun. 2019.

[18] H. Zimmermann, M. Zebisch, and N. Sträter, “Cellular function and molecular structure of ecto-nucleotidases.,” *Purinergic signalling*, vol. 8, no. 3, pp. 437–502, Sep. 2012.

[19] M. Matyash, O. Zabiegalov, S. Wendt, V. Matyash, and H. Kettenmann, “The adenosine generating enzymes CD39/CD73 control microglial processes ramification in the mouse brain.,” *PloS one*, vol. 12, no. 4, p. e0175012, 2017.

[20] I. Grković, D. Drakulić, J. Martinović, and N. Mitrović, “Role of Ectonucleotidases in Synapse Formation During Brain Development: Physiological and Pathological Implications.,” *Current neuropharmacology*, vol. 17, no. 1, pp. 84–98, 2019.

[21] I. Grković, N. Mitrović, M. Dragić, M. Adžić, D. Drakulić, and N. Nedeljković, “Spatial Distribution and Expression of Ectonucleotidases in Rat Hippocampus After Removal of Ovaries and Estradiol Replacement,” *Molecular Neurobiology*, vol. 56, no. 3, pp 1933-1945, Jul. 2019.

[22] G. Burnstock, “Purinergic Signalling: Therapeutic Developments.,” *Frontiers in pharmacology*, vol. 8, p. 661, 2017.

[23] L. Antonioli, P. Pacher, E. S. Vizi, and G. Haskó, “CD39 and CD73 in immunity and inflammation.,” *Trends in molecular medicine*, vol. 19, no. 6, pp. 355–367, Jun. 2013.

[24] M. C. Geloso, V. Corvino, and F. Michetti, “Trimethyltin-induced hippocampal degeneration as a tool to investigate neurodegenerative processes.,” *Neurochemistry international*, vol. 58, no. 7, pp. 729–738, Jun. 2011.

[25] A. Trabucco *et al.*, “Methylated tin toxicity a reappraisal using rodents models.,” *Archives italiennes de biologie*, vol. 147, no. 4, pp. 141–153, Dec. 2009.

[26] V. Corvino *et al.*, “Estrogen administration modulates hippocampal GABAergic subpopulations in the hippocampus of trimethyltin-treated rats.,” *Frontiers in cellular neuroscience*, vol. 9, p. 433, 2015.

[27] W. Lattanzi, V. Corvino, V. Di Maria, F. Michetti, and M. C. Geloso, “Gene expression profiling as a tool to investigate the molecular machinery activated during hippocampal neurodegeneration induced by

trimethyltin (TMT) administration.," *International journal of molecular sciences*, vol. 14, no. 8, pp. 16817–16835, Aug. 2013.

[28] M. Dragić, M. Zarić, N. Mitrović, N. Nedeljković, and I. Grković, "Two Distinct Hippocampal Astrocyte Morphotypes Reveal Subfield-Different Fate during Neurodegeneration Induced by Trimethyltin Intoxication.," *Neuroscience*, vol. 423, pp. 38–54, Dec. 2019.

[29] L. Latini *et al.*, "Trimethyltin intoxication up-regulates nitric oxide synthase in neurons and purinergic ionotropic receptor 2 in astrocytes in the hippocampus.," *Journal of neuroscience research*, vol. 88, no. 3, pp. 500–509, Feb. 2010.

[30] S. Haga, C. Haga, T. Aizawa, and K. Ikeda, "Neuronal degeneration and glial cell-responses following trimethyltin intoxication in the rat.," *Acta neuropathologica*, vol. 103, no. 6, pp. 575–582, Jun. 2002.

[31] A. R. Little, D. B. Miller, S. Li, M. L. Kashon, and J. P. O'Callaghan, "Trimethyltin-induced neurotoxicity: gene expression pathway analysis, q-RT-PCR and immunoblotting reveal early effects associated with hippocampal damage and gliosis.," *Neurotoxicology and teratology*, vol. 34, no. 1, pp. 72–82, 2012.

[32] N. Mitrović *et al.*, "Regional and sex-related differences in modulating effects of female sex steroids on ecto-5'-nucleotidase expression in the rat cerebral cortex and hippocampus.," *General and comparative endocrinology*, vol. 235, pp. 100–107, Sep. 2016.

[33] N. Mitrović *et al.*, "17β-Estradiol-Induced Synaptic Rearrangements Are Accompanied by Altered Ectonucleotidase Activities in Male Rat Hippocampal Synaptosomes.," *Journal of molecular neuroscience : MN*, vol. 61, no. 3, pp. 412–422, Mar. 2017.

[34] M. Dragić, M. Zarić, N. Mitrović, N. Nedeljković, and I. Grković, "Application of Gray Level Co-Occurrence Matrix Analysis as a New Method for Enzyme Histochemistry Quantification," *Microscopy and Microanalysis*, 2019.

[35] K. W. Dunn, M. M. Kamocka, and J. H. McDonald, "A practical guide to evaluating colocalization in biological microscopy.," *American journal of physiology. Cell physiology*, vol. 300, no. 4, pp. C723-42, Apr. 2011.

[36] S. Tsutsumi, M. Akaike, H. Arimitsu, H. Imai, and N. Kato, "Circulating corticosterone alters the rate of neuropathological and behavioral changes induced by trimethyltin in rats.," *Experimental neurology*, vol. 173, no. 1, pp. 86–94, Jan. 2002.

[37] F. Jauregui-Huerta, Y. Ruvalcaba-Delgadillo, R. Gonzalez-Castañeda, J. Garcia-Estrada, O. Gonzalez-Perez, and S. Luquin, "Responses of glial cells to stress and glucocorticoids.," *Current immunology reviews*, vol. 6, no. 3, pp. 195–204, Aug. 2010.

[38] B. S. Carter, D. E. Hamilton, and R. C. Thompson, "Acute and chronic glucocorticoid treatments regulate astrocyte-enriched mRNAs in multiple brain regions in vivo.," *Frontiers in neuroscience*, vol. 7, p.

139, 2013.

[39] C. D. Balaban, J. P. O'Callaghan, and M. L. Billingsley, "Trimethyltin-induced neuronal damage in the rat brain: comparative studies using silver degeneration stains, immunocytochemistry and immunoassay for neuronotypic and gliotypic proteins.," *Neuroscience*, vol. 26, no. 1, pp. 337–361, Jul. 1988.

[40] A. Verkhratsky, J. J. Rodrigues, A. Pivoriunas, R. Zorec, and A. Semyanov, "Astroglial atrophy in Alzheimer's disease.," *Pflugers Archiv : European journal of physiology*, vol. 471, no. 10, pp. 1247–1261, Oct. 2019.

[41] L. Erb, L. T. Woods, M. G. Khalafalla, and G. A. Weisman, "Purinergic signaling in Alzheimer's disease.," *Brain research bulletin*, vol. 151, pp. 25–37, Sep. 2019.

[42] M. Cieślak and A. Wojtczak, "Role of purinergic receptors in the Alzheimer's disease.," *Purinergic signalling*, vol. 14, no. 4, pp. 331–344, Dec. 2018.

[43] N. Braun *et al.*, "Assignment of ecto-nucleoside triphosphate diphosphohydrolase-1/cd39 expression to microglia and vasculature of the brain.," *The European journal of neuroscience*, vol. 12, no. 12, pp. 4357–4366, Dec. 2000.

[44] F. Hao *et al.*, "Chemokine fractalkine attenuates overactivation and apoptosis of BV-2 microglial cells induced by extracellular ATP.," *Neurochemical research*, vol. 38, no. 5, pp. 1002–1012, May 2013.

[45] F. L. Heppner, K. Roth, R. Nitsch, and N. P. Hailer, "Vitamin E induces ramification and downregulation of adhesion molecules in cultured microglial cells.," *Glia*, vol. 22, no. 2, pp. 180–188, Feb. 1998.

[46] M. A. Wollmer, R. Lucius, H. Wilms, J. Held-Feindt, J. Sievers, and R. Mentlein, "ATP and adenosine induce ramification of microglia in vitro.," *Journal of neuroimmunology*, vol. 115, no. 1–2, pp. 19–27, Apr. 2001.

[47] D. Boche, V. H. Perry, and J. A. R. Nicoll, "Review: activation patterns of microglia and their identification in the human brain.," *Neuropathology and applied neurobiology*, vol. 39, no. 1, pp. 3–18, Feb. 2013.

[48] W. Y. Tam and C. H. E. Ma, "Bipolar/rod-shaped microglia are proliferating microglia with distinct M1/M2 phenotypes.," *Scientific reports*, vol. 4, p. 7279, Dec. 2014.

[49] A. G. Orr, A. L. Orr, X.-J. Li, R. E. Gross, and S. F. Traynelis, "Adenosine A(2A) receptor mediates microglial process retraction.," *Nature neuroscience*, vol. 12, no. 7, pp. 872–878, Jul. 2009.

[50] K. Ohsawa, T. Sanagi, Y. Nakamura, E. Suzuki, K. Inoue, and S. Kohsaka, "Adenosine A3 receptor is involved in ADP-induced microglial process extension and migration.," *Journal of neurochemistry*, vol. 121, no. 2, pp. 217–227, Apr. 2012.

[51] S. Koizumi *et al.*, “UDP acting at P2Y6 receptors is a mediator of microglial phagocytosis.,” *Nature*, vol. 446, no. 7139, pp. 1091–1095, Apr. 2007.

[52] M. Adzic and N. Nedeljkovic, “Unveiling the Role of Ecto-5’-Nucleotidase/CD73 in Astrocyte Migration by Using Pharmacological Tools.,” *Frontiers in pharmacology*, vol. 9, p. 153, 2018.

[53] C. J. Ferrante *et al.*, “The adenosine-dependent angiogenic switch of macrophages to an M2-like phenotype is independent of interleukin-4 receptor alpha (IL-4Rα) signaling.,” *Inflammation*, vol. 36, no. 4, pp. 921–931, Aug. 2013.

[54] M. Jakovljevic *et al.*, “Induction of NTPDase1/CD39 by Reactive Microglia and Macrophages Is Associated With the Functional State During EAE.,” *Frontiers in neuroscience*, vol. 13, p. 410, 2019.

[55] M. Ramanathan *et al.*, “Differential regulation of HIF-1alpha isoforms in murine macrophages by TLR4 and adenosine A(2A) receptor agonists.,” *Journal of leukocyte biology*, vol. 86, no. 3, pp. 681–689, Sep. 2009.

[56] G. Pinhal-Enfield *et al.*, “An angiogenic switch in macrophages involving synergy between Toll-like receptors 2, 4, 7, and 9 and adenosine A(2A) receptors.,” *The American journal of pathology*, vol. 163, no. 2, pp. 711–721, Aug. 2003.

[57] F. Di Virgilio, “Liaisons dangereuses: P2X(7) and the inflammasome.,” *Trends in pharmacological sciences*, vol. 28, no. 9, pp. 465–472, Sep. 2007.

[58] S. Viana da Silva *et al.*, “Early synaptic deficits in the APP/PS1 mouse model of Alzheimer’s disease involve neuronal adenosine A2A receptors.,” *Nature communications*, vol. 7, p. 11915, Jun. 2016.

[59] E. Faivre *et al.*, “Beneficial Effect of a Selective Adenosine A(2A) Receptor Antagonist in the APPswe/PS1dE9 Mouse Model of Alzheimer’s Disease.,” *Frontiers in molecular neuroscience*, vol. 11, p. 235, 2018.

[60] A. Delekate, M. Füchtemeier, T. Schumacher, C. Ulbrich, M. Foddis, and G. C. Petzold, “Metabotropic P2Y1 receptor signalling mediates astrocytic hyperactivity in vivo in an Alzheimer’s disease mouse model.,” *Nature communications*, vol. 5, p. 5422, Nov. 2014.

[61] N. Reichenbach *et al.*, “P2Y1 receptor blockade normalizes network dysfunction and cognition in an Alzheimer’s disease model.,” *The Journal of experimental medicine*, vol. 215, no. 6, pp. 1649–1663, Jun. 2018.

[62] D. O. Borroto-Escuela, S. Hinz, G. Navarro, R. Franco, C. E. Müller, and K. Fuxe, “Understanding the Role of Adenosine A2AR Heteroreceptor Complexes in Neurodegeneration and Neuroinflammation.,” *Frontiers in neuroscience*, vol. 12, p. 43, 2018.

Tables

Table 1. List of antibodies

Antibody	Source and Type	Used dilution	Manufacturer
Iba-1	Goat, polyclonal	1:400 IHC, IF	Abcam ab5076, RRID:AB_2224402
CD73, rNu-9L(I4,I5)	Rabbit, polyclonal	1:300 IHC, IF	Ectonucleotidases-ab.com
CD39, mN1-2C(I4,I5)	Guinea pig, polyclonal	1:200 IF	Ectonucleotidases-ab.com
Arg-1	Rabbit, polyclonal	1:200 IF	Sigma AV45673, RRID:AB_1844986
iNOS	Rabbit, polyclonal	1:200 IF	Abcam ab15323, RRID:AB_301857
CD68	Rabbit, polyclonal	1:200 IF	Abcam ab125212, RRID:AB_10975465
$P2Y_{12}$	Rabbit, polyclonal	1:300 IF	Sigma P4817, RRID:AB_261954
GFAP	Mouse, monoclonal	1:100 IF	UC Davis/NIH NeuroMab Facility (73–240), RRID:AB_10672298
GFAP	Rabbit, polyclonal	1:100 IF	UC Davis/NIH NeuroMab Facility (73–240), RRID:AB_10672298
Amyloid β 42	Rabbit, monoclonal	1:500 IHC, IF	Invitrogen 700254, RRID: AB_2532306
GFAP	Rabbit, polyclonal	1:500 IF	DAKO, Agilent Z0334, RRID:AB_10013382
C3	Goat, polyclonal	1:300 IF	Thermo Fisher Scientific PA1-29715 RRID: AB_AB_2066730
TNF-α	Goat, polyclonal	1:100 IF	Santa Cruz Biotechnology, sc-1350, RRID: AB_2204365
IL-10	Goat, polyclonal	1:100 IF	Santa Cruz Biotechnology, sc-1783, RRID: AB_2125115
NF-kB	Rabbit, polyclonal	1:100 IF	Santa Cruz Biotechnology, sc-109, RRID: AB_632039
IL-1β/IL-1F2	Goat, polyclonal	1:100 IF	R&D Systems, AF-501-NA, RRID: AB_ 354508
$P2Y_1$	Rabbit, polyclonal	1:300 IF	Alomone Labs; APR-0009, RRID: AB_2040070
A_{2A}	Rabbit, polyclonal	1:300 IF	Abcam, ab3461, RRID: AB_303823

Anti-mouse IgG Alexa Fluor 488	Donkey, polyclonal	1:400 IF	Invitrogen A21202, RRID:AB_141607
Anti-goat IgG Alexa Fluor 488	Donkey, polyclonal	1:400 IF	Invitrogen A-11055, RRID:AB_142672
Anti-rabbit IgG Alexa Fluor 555	Donkey, polyclonal	1:400 IF	Invitrogen A-21428, RRID:AB_141784
Anti-mouse IgG Alexa Fluor 647	Donkey, polyclonal	1:400 IF	Thermo Fisher Scientific A-31571, RRID:AB_162542
Anti-goat HRP-conjugated IgG	Rabbit, polyclonal	1:200 IHC	R&D Systems, HAF017 RRID:AB_56258
Anti-rabbit IgG Alexa Fluor 488	Donkey, polyclonal	1:400 IF	Invitrogen A-21206, RRID:AB_141708
Anti – guinea pig IgG Alexa Fluor 555	Goat, polyclonal	1:200 IF	Invitrogen A-21435, RRID:AB_2535856
Anti-mouse HRP-conjugated IgG	Goat, polyclonal	1:200 IHC	R&D Systems, HAF007 RRID:AB_562588
Anti-goat HRP-conjugated IgG	Rabbit, polyclonal	1:200 IHC	R&D Systems, HAF017 RRID:AB_56258

Table 2. Primer sequences used for RT-qPCR

Gene	Sequence (5'- -3')	Length (bp)
NTPDase1 (*Entpd1*)	TCAAGGACCCGTGCTTTTAC	150
	TCTGGTGGCACTGTTCGTAG	
eN (*Nt5e*)	CAAATCTGCCTCTGGAAAGC	160
	ACCTTCCAGAAGGACCCTGT	
$P2X_4R$ (*P2rx4*)	ACCAGGAAACGGACTCTGTG	168
	TCACGGTGACGATCATGTTGG	
$P2X_7R$ (*P2rx7*)	ATTGTTAGGCCAATGGCAAG	190
	AACACCTTCACCGTCTCCAC	
$P2Y_2R$ (*P2ry2*)	TCACCCGCACCCTCTATTAC	139
	GCCAGGAAGTAGAGCACAGG	
$P2Y_6R$ (*P2ry6*)	CAGTTATGGAGCGGGACAAT	104
	GTAAACTGGGGGTAGCAGCA	
$P2Y_{12}R$ (*P2ry12*)	CGAAACCAAGTCACTGAGAGGA	162
	CCAGGAATGGAGGTGGTGTTG	
A_1R (*Adora1*)	GTGATTTGGGCTGTGAAGGT	194
	GAGCTCTGGGTGAGGATGAG	
$A_{2A}R$ (*Adora2a*)	TGCAGAACGTCACCAACTTC	141
	CAAAACAGGCGAAGAAGAGG	
$A_{2B}R$ (*Adora2b*)	CGTCCCGCTCAGGTATAAAG	104
	CCAGGAAAGGAGTCAGTCCA	
A_3R (*Adora3*)	TTCTTGTTTGCCTTGTGCTG	129
	AGGGTTCATCATGGAGTTCG	
IL-1β (*Il1b*)	CACCTCTCAAGCAGAGCACAG	79
	GGGTTCCATGGTGAAGTCAAC	
TNFα (*Tnf*)	CCCCCATTACTCTGACCCCT	88
	CCCAGAGCCACAATTCCCTT	
IL-6 (*Il6*)	CCGGAGAGGAGACTTCACAG	160
	ACAGTGCATCATCGCTGTTC	
IL-10 (*Il10*)	GCTCAGCACTGCTATGTTGC	106

	GTCTGGCTGACTGGGAAGTG	
C3 (*C3*)	GCGGTACTACCAGACCATCG CTTCTGGCACGACCTTCAGT	166
iNOS (*Nos2*)	ACACAGTGTCGCTGGTTTGA AACTCTGCTGTTCTCCGTGG	125
Arg1 (*Arg1*)	CTGTGGTAGCAGAGACCCAGA GGTTGTCAGCGGAGTGTTGA	161
CyCA (*Ppia*)	CAAAGTTCCAAAGACAGCAGAAAA CCACCCTGGCACATGAAT	114

Figures

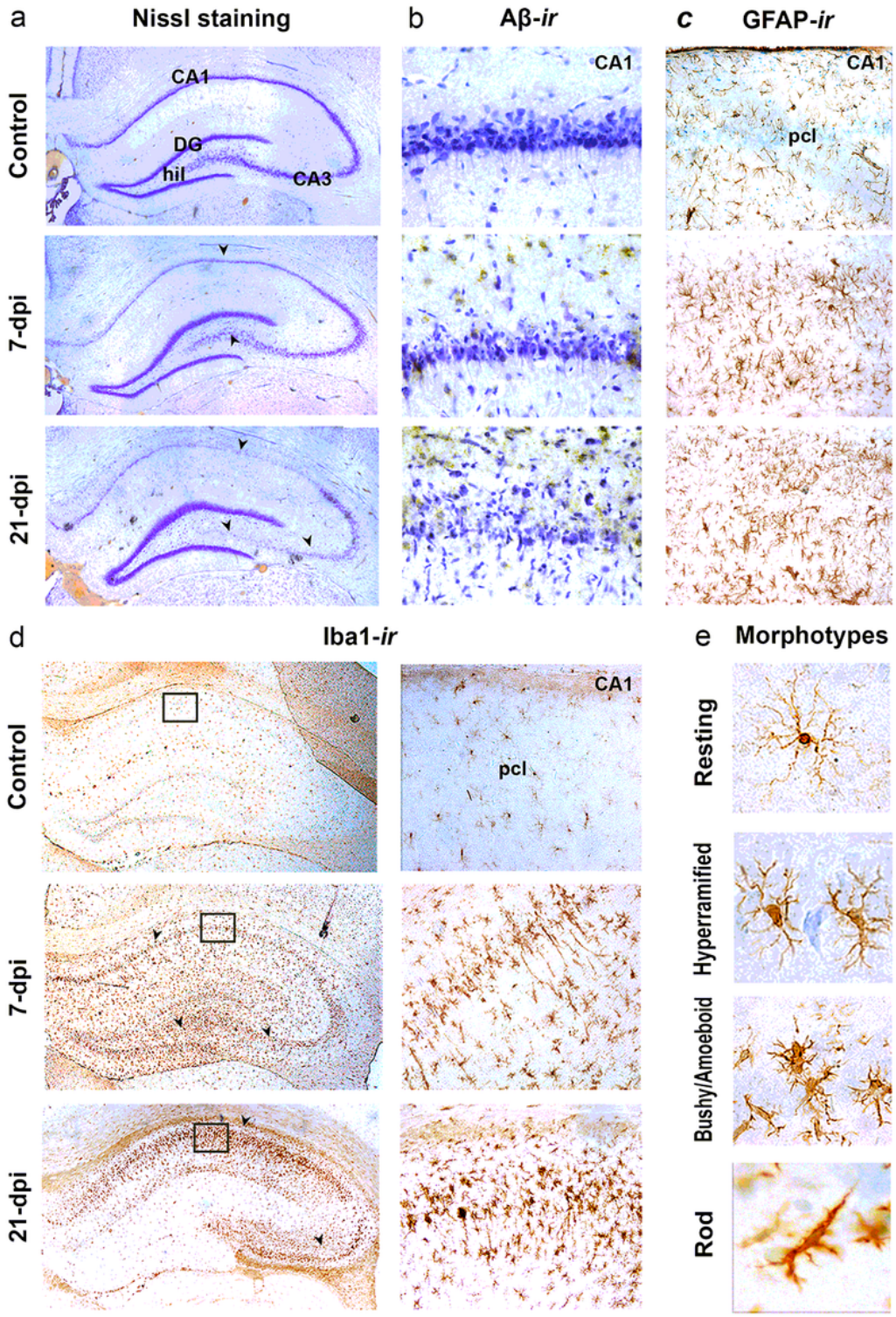

Figure 1

Spatio-temporal pattern of hippocampal neurodegeneration, amyloid-β deposition and gliosis after TMT exposure. (a) Thionine staining of 25-µm thick coronal sections, obtained from control animal and at 7-dpi and 21-dpi after TMT exposure, captured under the light microscope under 5× magnification. Arrowheads point to neuronal cell layers with noticeable cell death. Rectangular shows position of the CA2 sector. (b) Immunohistochemical detection of Aβ depositions in the hippocampal CA1 sector in

control sections and at 7-dpi and 21-dpi. Micrographs were captured under 20× magnification. (c) Immunohistochemical staining of GFAP showing CA1 sector in control animal and at 7-dpi and 21-dpi captured under 20× magnification. (d). Immunohistochemical staining of Iba1, showing whole hippocampal area under 5× magnification and the corresponding enlarged areas captured under 20× magnification in control animals at 7-dpi and 21-dpi. (e) Distinct microglial morphotypes observed by Iba1-immunostaining in the hippocampal areas, and captured under 63× magnification.

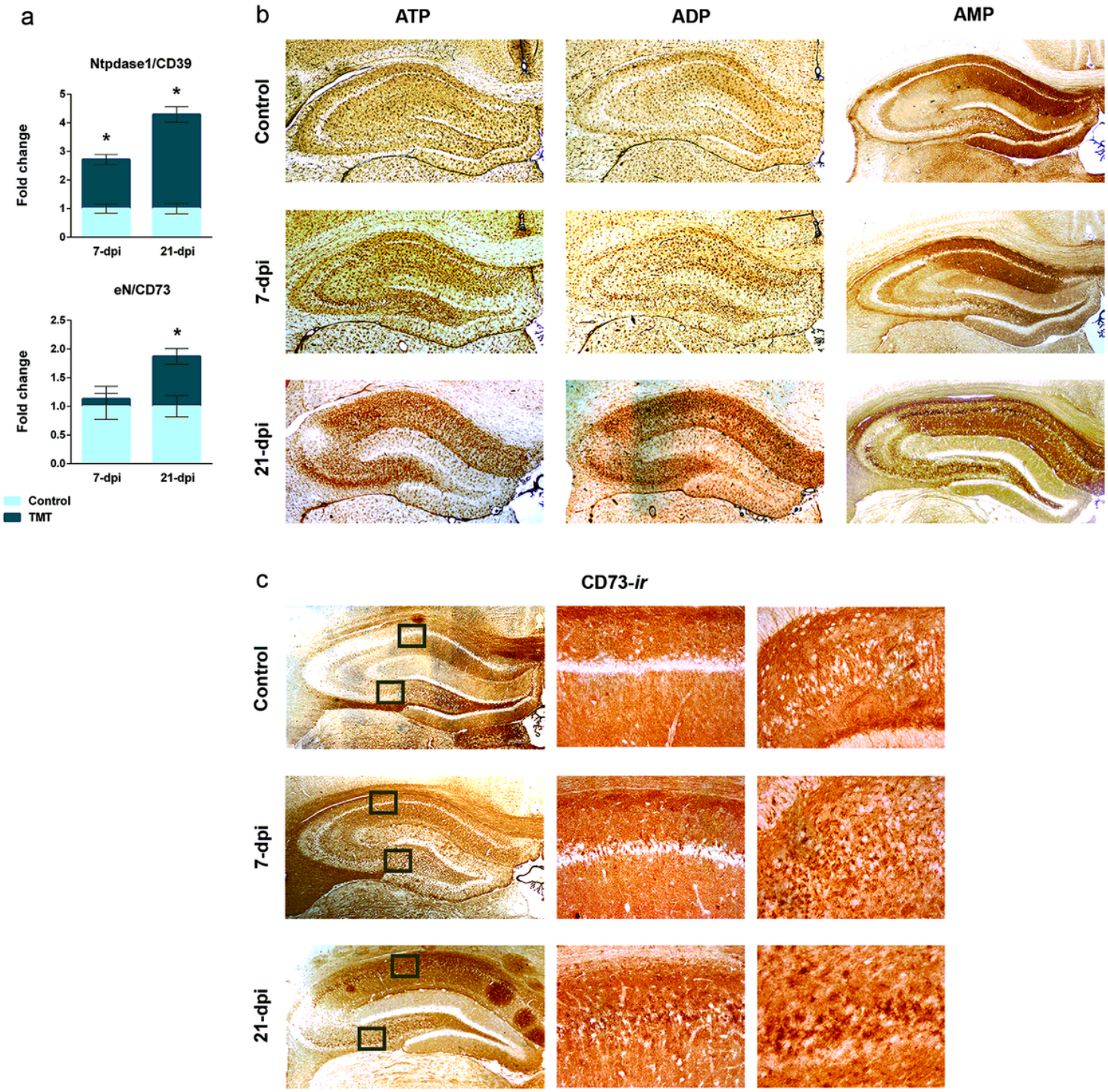

Figure 2

Expression of NTPDase1/CD39 and eN/CD73 in the hippocampal region after TMT exposure. (a) RT-qPCR analysis of genes encoding NTPDase1/CD39 and eN/CD73 in the hippocampal tissue. Bars represent mean fold change in target gene/CycA-mRNA abundance (dark green) relative to intact control (light green) ±.SD. Level of significance - *p 0.05. (b) ATPase-, ADPase- and AMPase-based histochemistry, labeling cells and structures that exhibit the corresponding ectonucleotidase activities in the hippocampal region. Micrographs captured under 5× magnification. (c). Immunohistochemical staining of eN/CD73 in the hippocampal region at control section and at 7-dpi and 21-dpi. Rectangles show areas captured and presented at higher (20×) magnification.

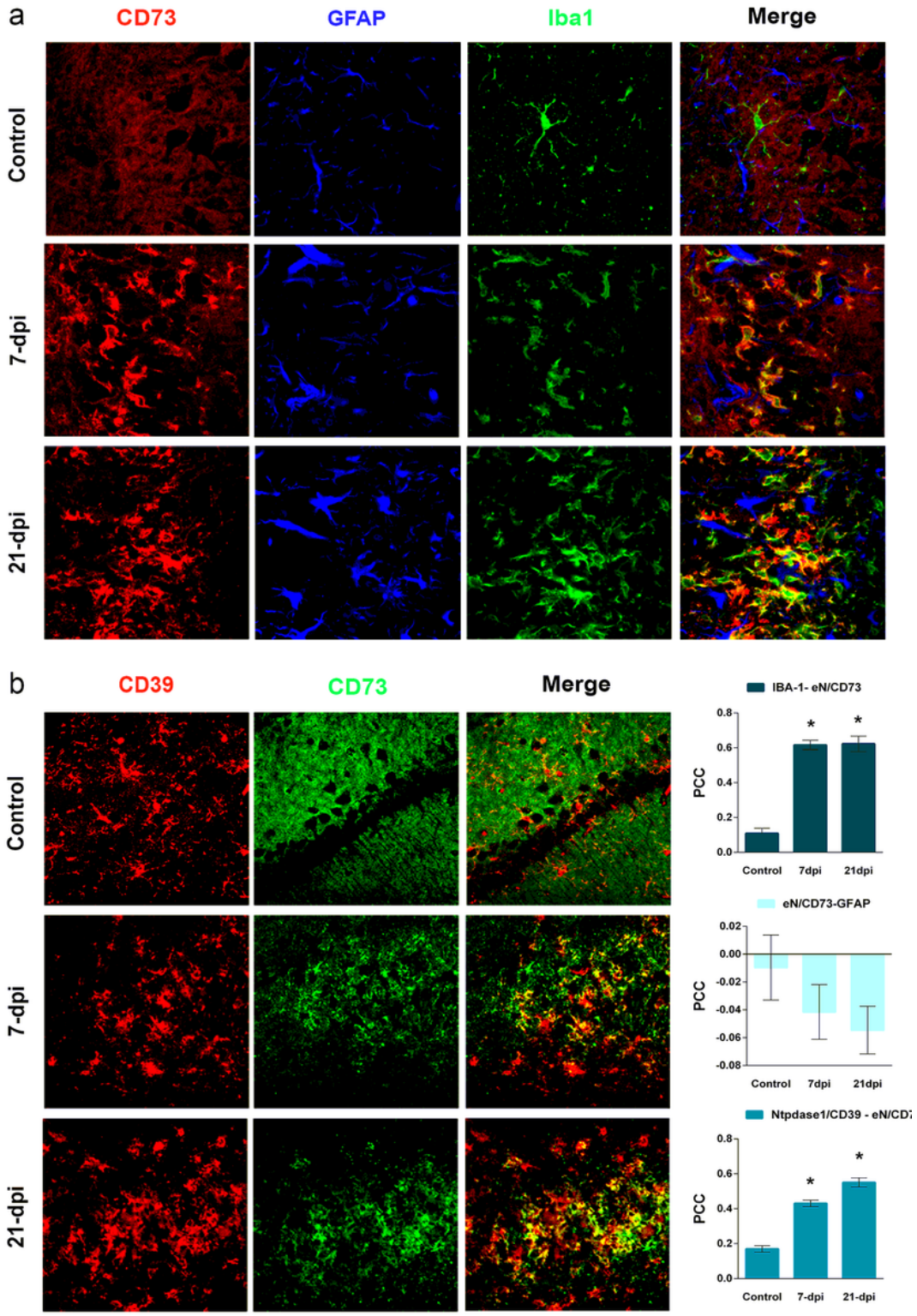

Figure 3

Identification of cells that upregulate eN/CD73 after TMT exposure. (a) Triple immunofluorescence labeling directed to eN/CD73 (red), astrocyte marker GFAP (blue) and microglial marker Iba1 (green), showing the overlapping signal (merge) corresponding to Iba1-ir and eN/CD73-ir at control, 7-dpi and 21-dpi. (b) Double immunofluorescence labeling directed to NTPDase1/CD39 (red) and eN/CD73 (green), showing the overlapping signals (merge) at control section and at 7-dpi and 21-dpi. (c) Pearson

correlation coefficients (PCC) indicating the level of signal overlap between Iba1-ir and eN/CD73-ir, eN/CD73-ir and GFAP-ir and NTPDase1/CD39-ir and eN/CD73-ir. Bars show mean PCC ± SEM, from 3 ROI selected from 5 sections. Level of significance - *p □ 0.05.

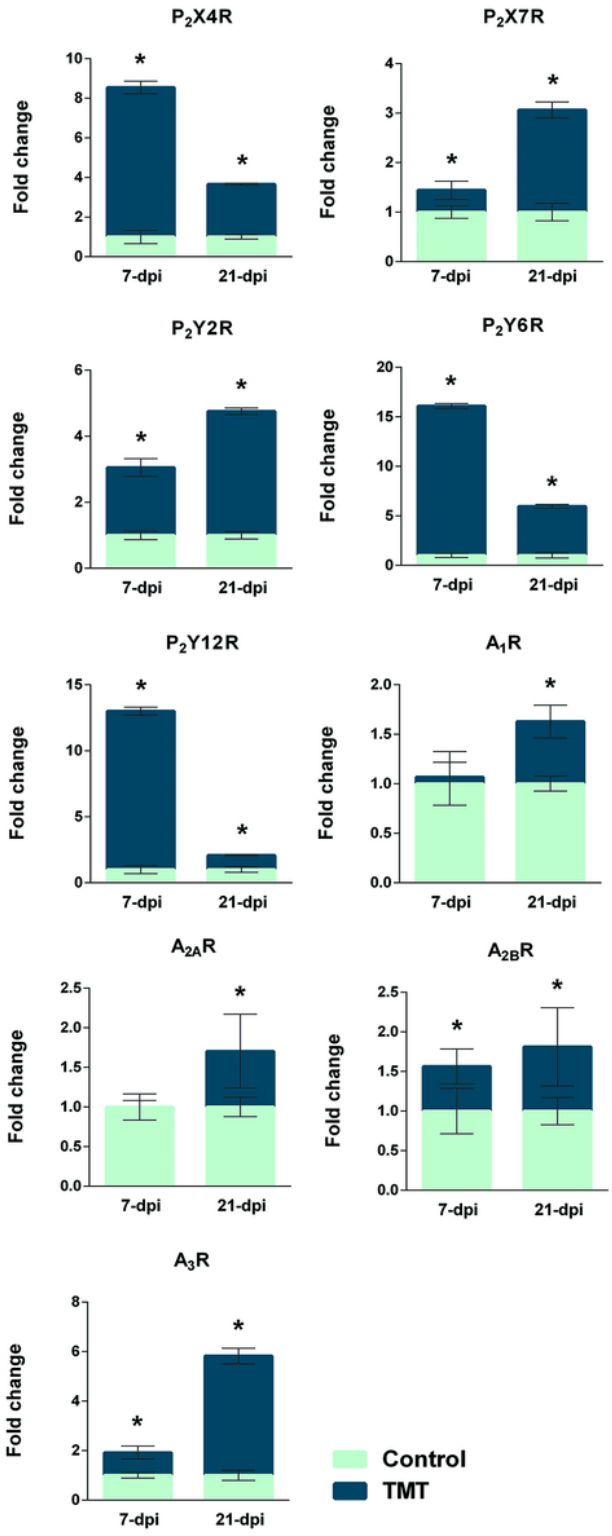

Figure 4

Purinoceptors gene expression. The abundances of transcripts coding for P2X4, P2X7, P2Y2R, P2Y6R, P2Y12R, A1R, A2AR, A2BR and A3R were assessed by RT-qPCR. Bars represent mean fold change in

target gene/CycA-mRNA (dark green) in respect to intact control (light green) ± SD. Level of significance - *p 0.05.

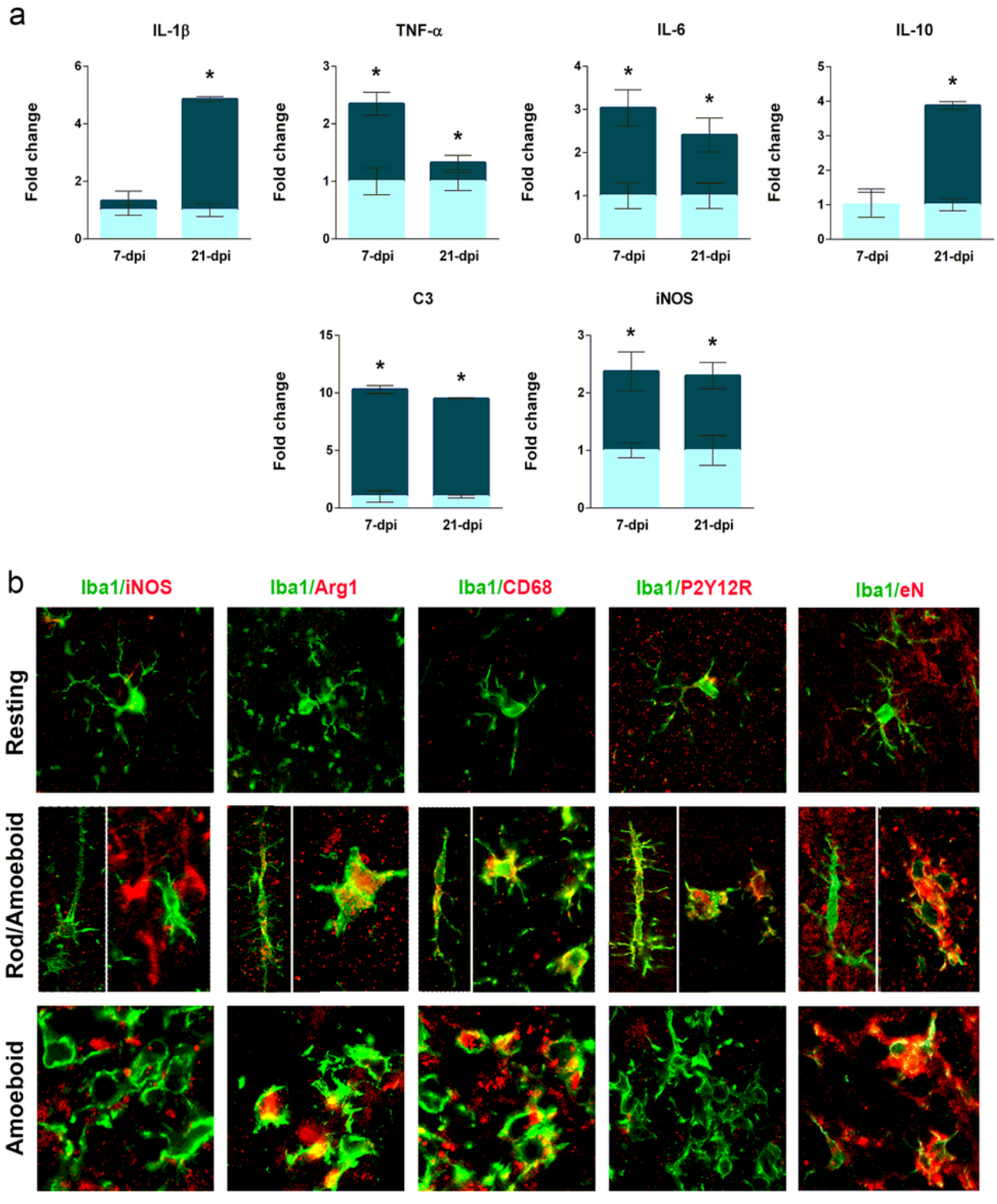

Figure 5

Assessment of functional state of reactive microglia after TMT exposure. (a) The abundance of transcripts coding IL-1β, TNF-α, IL-6, IL-10, C3 and iNOS. Bars represent mean fold change in target gene/CycA-mRNA (dark green) in respect to intact control (light green) ± SD. Level of significance - *p

0.05. (b) Iba1-immunofluorescence combined with second immunofluorescence labeling directed to iNOS, Arg1, CD68 and P2Y12, showing Iba1-ir cells that expressed Arg1, CD68 and P2Y12 -ir. Rod and amoeboid microglia shown at 7-dpi at 63× magnification.

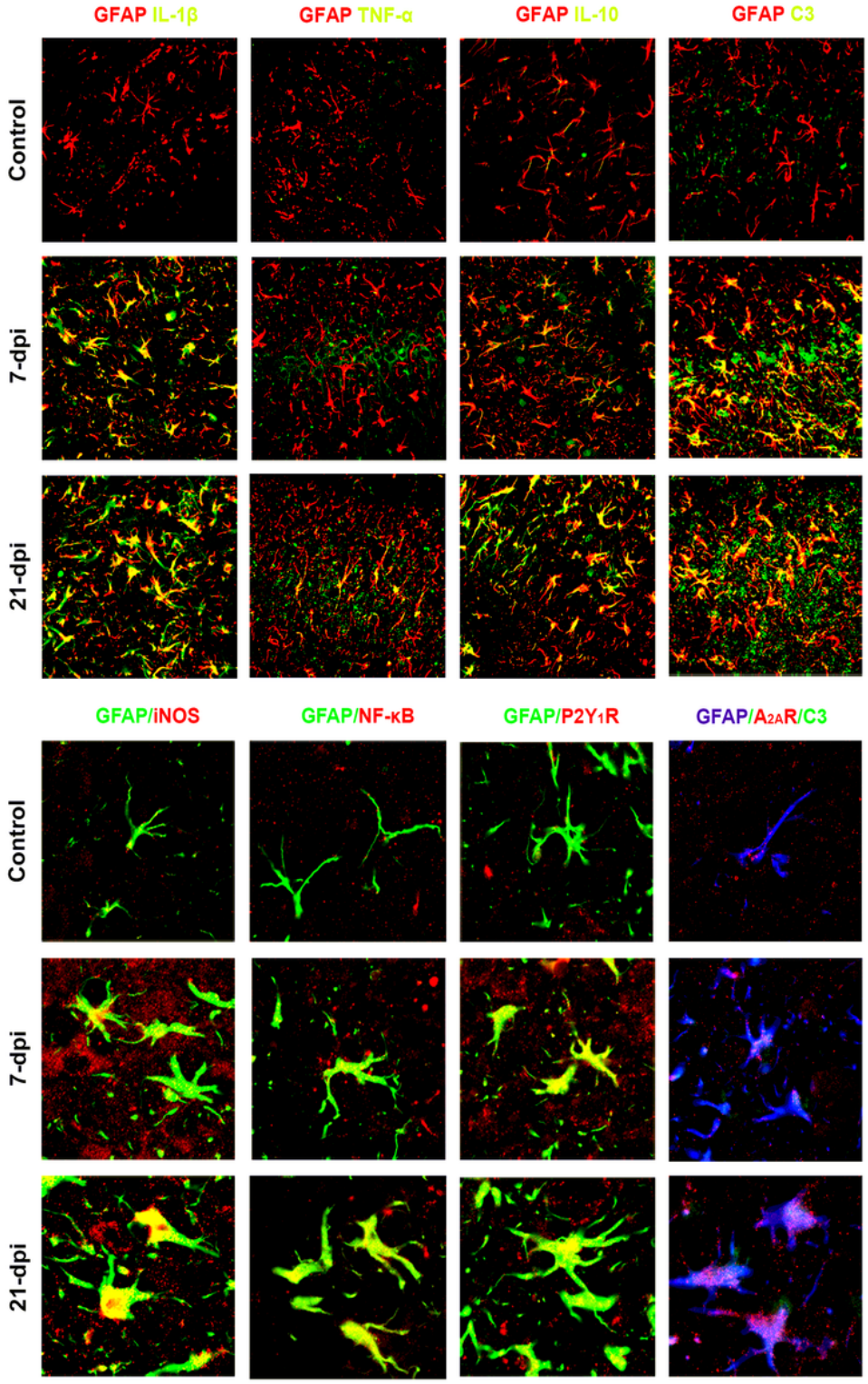

Figure 6

Assessment of functional state of reactive astrocytes after TMT exposure. GFAP-immunofluorescence combined with second immunofluorescence labeling directed to IL-1β, TNF-α, IL-10 and C3, iNOS, NF-kB

and P2Y1R. Triple immunofluorescence labeling directed to GFAP, C3 and A2AR. Micrographs were captured under 40× and 63× magnification.

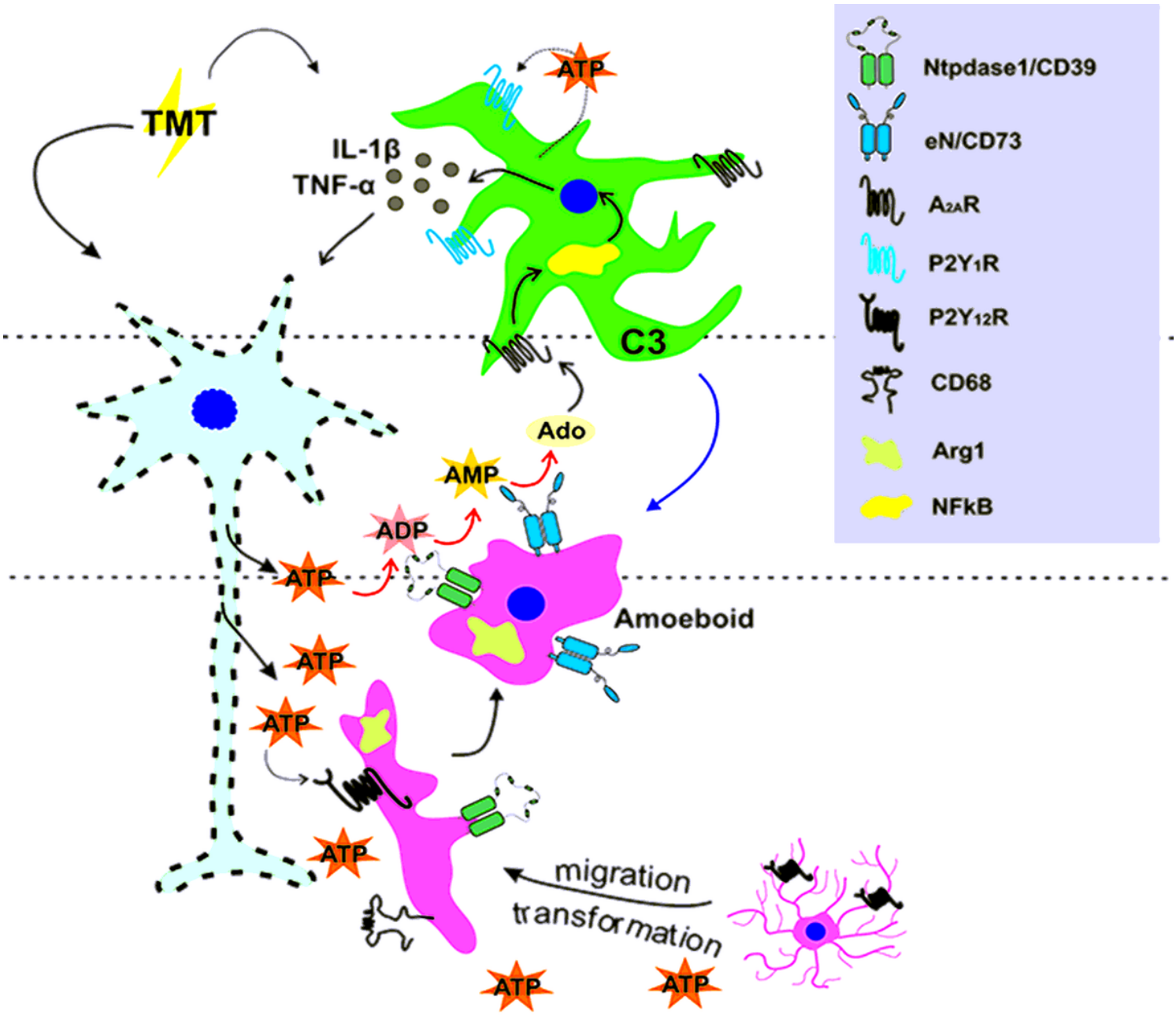

Figure 7

Proposed model of purinergic signaling component interactions in molecular events underlying trimethyltin-induced neurodegeneration An initial pathologic event occurs (TMT), causing damage to pyramidal and granular neurons of hippocampus. Damaged neurons release ATP as a DAMP molecule, which attracts microglia to the site of neurodegeneration via P2Y12R. ATP is degraded to adenosine via CD39/CD73 enzymes co-expressed on reactive, amoeboid microglia. Damaged neurons as well as TMT activates astrocytes, which express pro-inflammatory factors. Furthermore, we found increased astrocytic A2AR and P2Y1R expression. ATP and CD73-derived adenosine activate A2AR/P2Y1R, which might contribute to chronic astrocyte activation and its pro-inflammatory phenotype.

Supplementary Files

This is a list of supplementary files associated with this preprint. Click to download.

- Supplementarytable1.docx